COBEM 2023 27TH INTERNATIONAL CONGRESS OF MECHANICAL ENGENEERING

ABCM Brazilian Society of Mechanical Sciences and Engineering
27th ABCM International Congress of Mechanical Engineering
December 04-08, 2023, Florianópolis-SC, Brazil

COB-2023-1024

MANUFACTURING AND CHARACTERIZATION OF A CERAMIC COMPOSITE Al_2O_3-ZrO_2-SiC_w SINTERED BY PECS

Luma Gonçalves Fraga
Federal University of Espírito Santo, Mechanical Engineering Department, 29075-910, Vitória/ES, Brazil
luma.fraga@edu.ufes.br

Izabel Fernanda Machado
University of Sao Paulo, Polytechnic School, Department of Mechatronic Engineering and Mechanical Systems, 05508-900, São Paulo/SP, Brazil
machadoi@usp.br

Marcelo Bertolete Carneiro
Federal University of Espírito Santo, Mechanical Engineering Department, 29075-910, Vitória/ES, Brazil
marcelo.b.carneiro@ufes.br

Abstract. *Cutting tools must remain hard and tough at elevated temperatures to withstand fracture and wear. Among the materials that can be used as cutting tools, alumina (Al_2O_3) based ceramics stand out. They are recognized for their intrinsic properties, such as high melting point, low thermal conductivity, and good chemical inertia. However, despite their high hardness and wear resistance, they have low fracture toughness. The addition of second phase, fiber matrix reinforcement, and stress-induced phase transformation are methods to increase the fracture toughness in these materials. This work aims to manufacture and characterize an advanced ceramic sample made of ultrafine powder of α-Al_2O_3, nanopowder of Y-ZrO_2 and fine powder of β-SiC_w fibers. The sample was sintered by pulsed electric current sintering (PECS) with axial pressure application of 50 MPa, dwell temperature of 1500°C, working cycle of 36 minutes, and vacuum atmosphere. X-ray diffraction (XRD) analysis was performed on the mixed powders, in addition to the sintered sample. The experimental density was evaluated using Archimedes' principle. Scanning electron microscopy (SEM) and energy-dispersive X-ray spectroscopy (EDS) were performed on the surface of the longitudinal section to observe the different phases. The mechanical properties, hardness and fracture toughness, were also assessed. The ceramic sample achieved a relative density of 95.83 ± 0.47%. The Vickers hardness number was 1718.25 ± 118.02 HV10, while the fracture toughness was 3.69 ± 0.57 MPa.$m^{1/2}$. The results indicated the viability of manufacturing Al_2O_3-based ceramics by PECS with good densification, and mechanical properties in a short time.*

Keywords: *Al_2O_3, PECS, density, hardness, fracture toughness.*

1. INTRODUCTION

Machining is a manufacturing process that aims to give shape and finishing to parts with the assistance of cutting tools. For this purpose, those tools must have properties to withstand the loads without deformation or fracture (Ranjan and Hiremath, 2019; Moghanlou *et al.*, 2019). Among the cutting tool materials, alumina-based ceramics (Al_2O_3) stand out because of their high hardness, and wear resistance, even at elevated temperatures, in addition to their chemical inertness (Chen *et al.*, 2015; Fang *et al.*, 2019). Owing to intrinsic properties, related to ionic and covalent bondings, structural ceramics are considered brittle, exhibiting low fracture toughness (Chen *et al.*, 2015; Otitoju *et al.*, 2020).

There are some toughening mechanisms to improve fracture toughness in advanced ceramics, such as the addition of a second-phase, fiber matrix reinforcement, and stress-induced phase transformation (Gong *et al.*, 2018; Zhang *et al.*, 2020). Fang *et al.* (2019) reported the use of whiskers such as silicon carbide (SiC_w) and yttria-stabilized zirconia (Y-ZrO_2) as Al_2O_3 toughening materials.

SiC whiskers have been reported in the literature as a fiber reinforcement in the alumina matrix because of their outstanding properties. Owing to their high hardness and Young's modulus, the crack is not able to break them easily. Thus, the main toughening mechanisms of whiskers are crack deflection, whisker bridging, and whisker pull-out. All those processes increase the fracture toughness by consuming the crack propagation energy (Chai *et al.*, 2020; Ma *et al.*, 2022). Zirconia presents polymorphic forms, when it is stabilized with small amounts of oxides, such as yttria; the tetragonal metastable phase occurs at room temperature. When cracking occurs, stresses at the crack tip may transform tetragonal to monoclinic zirconia. This change promotes an increase in the zirconia volume, which creates compressive stresses at

the crack tip, inhibiting its propagation along the material, increasing the fracture toughness (Boniecki *et al.*, 2017; Chai *et al.*, 2020).

Pulsed electric current sintering (PECS) is a sintering technique characterized by fast heating rate, short dwell time, short processing time, low sintering temperature, and controlled atmosphere by vacuum, activated and/or inert gas. It simultaneously applies electric current pulses and mechanical load through the die to consolidate the powder (Orru *et al.*, 2009; Grigoriev *et al.*, 2017).

Zhang *et al.* (2022) fabricated Al_2O_3-SiC_w-Si_3N_4-based ceramic material by PECS and compared it with hot-pressing (HP). They noticed PECS allowed a reduction of 100°C in the sintering temperature and even increased the sample properties. Furthermore, they submitted this sample to hardness and fracture toughness tests by changing the temperature from room to 1000°C. Both properties were found to decrease with increasing temperature, although even at 1000°C the hardness kept 67% of its value at room temperature.

Casto *et al.* (1997) evaluated wear rate and wear mechanisms of alumina-based tools (Al_2O_3–7vol%ZrO_2, Al_2O_3–TiN–TiC–ZrO_2, Al_2O_3–SiC_w) and cemented carbide tool (WC–TiC–Co) turning AISI 1040 steel at a low cutting speed. They reported adhesion and plastic deformation as wear mechanisms for zirconia-toughened alumina, mixed-based alumina and cemented carbide in the craters and cutting edges, in addition to adhesion and chipping wear mechanisms for whisker reinforced alumina. Zirconia-toughened alumina and mixed-based alumina ceramic tools had higher tool-life when compared with others.

Chen *et al.* (2015) investigated the SiC content and sintering temperature in Al_2O_3–mullite–ZrO_2–SiC composites manufactured by HP. The results indicated that when it was sintered at 1530°C with the addition of SiC around 20vol%, the Vickers hardness, flexural strength, and fracture toughness were improved. The increase in SiC content caused a slight increase in porosity.

Gevorkyan *et al.* (2020) fabricated an Al_2O_3-15%SiC insert using nanopowder by HP at 1600°C and investigated the performance of it and other alumina-based commercial cutting inserts, with additions of TiN, TiC and/or ZrO_2. They found that the Al_2O_3-15%SiC allowed increasing cutting speed when machining hardened steels, and the tool-life was longer than the other ceramics tools rehearsed.

Chakravarty and Sundararajan (2013) manufactured Al_2O_3–TiCN–ZrO_2 nanocomposites by PECS. They obtained better mechanical properties for a composition of around 23% of ZrO_2 and TiCN nanoparticles sintered at 1200°C. Using this sample as an insert, the results showed that the tool-life of the nanocomposite was higher than the commercial. Furthermore, the commercial tool failed by brittle fracture while the Al_2O_3–TiCN–ZrO_2 failed by abrasive wear at higher cutting speeds. The higher toughness of Al_2O_3–TiCN–ZrO_2 prevented the brittle fracture.

This work aims to manufacture and evaluate an alumina-based ceramic toughened with Y-ZrO_2 and reinforced with SiC_w. Thus, the powder metallurgy routine and pulsed electric current sintering were used to fabricate the sample. Relative density was evaluated using Archimedes' principle. Mechanical properties, such as hardness and fracture toughness were also assessed.

2. METHODOLOGY

2.1 Powder preparation and sintering

Aluminium oxide (α-Al_2O_3, 99.99% purity, 0.2 μm average particle size, 3.97 g/cm^3 density) mixed with zirconium oxide stabilized by 3 mol yttrium oxide (ZrO_2–3%$_{mol}$$Y_2O_3$, 99.5%, 0.04 μm, 5.84 g/cm^3) and fibers of silicon carbide whiskers (SiC_w, 99% purity, Ø 0.10 - 2.50 μm and 2.0 - 50 μmm length, 3.22 g/cm^3) were the powders used to compound the advanced ceramic sample.

The powders were mixed (70%volAl_2O_3-10vol%ZrO_2-20vol%SiC_w) in a liquid environment of isopropyl alcohol with austenitc stainless steel milling elements at a mass ratio of 6:1 (ball milling:powder) for 24 hours in a Wagner mixer (New Lab). Next, the mixture was dried in a laboratory drying oven (model NL80/42, New Lab) for about 24 hours at 50ºC and mechanically deagglomerated for 4 hours. The loose powder was manually deposited on a graphite die (MBIS60X, Morganite) which was internally covered by a graphite sheet (Grafoil GTB, Morganite) to avoid adhesion of the powders with the punches and die wall.

The sintering step occurred in a pulsed electric current sintering (PECS) machine (model SPS 1050, SPS Syntex Inc.), in a vacuum-controlled atmosphere of around 10 Pa. The heating and cooling rate was approximately 100ºC/min. The dwell temperature of 1500°C was held for 7 minutes, while a uniaxial pressure of 50 MPa was applied throughout the thermal cycle. The DC pulse pattern 12 On 2 Off with 3.3 ms/pulse was used.

2.2 Sample preparation

After sintering, the sample was sectioned on a precision saw (IsoMet 4000, Buehler) using a diamond wheel (15HC, Buehler). Half of it was used in the density and microscopic analysis, and the other half, in the mechanical tests.

To perform the microscopy and mechanical tests, metallographic preparation was needed. First, the sample was

mounted in phenolic thermoset resin using a manual compression-mounting machine (EFD 30, Fortel). The surface was grounded in a semi-automatic grinder-polisher (PFLDV, Fortel) using flat glass plates and SiC powders with grit sizes of #400, #600 and #1000 (Buehler). For the polishing step, nylon clothes (PSA, Buehler) with diamond pastes (MetaDi II, Buehler) having particle sizes of 15, 6 and 1 μm were used.

2.3 Microscopic and XRD characterization

The X-ray diffraction (XRD) analysis of the mixed powder was conducted in the diffractometer (Ultima IV, Rigaku), using a Mo monochromatic radiation, operating with a voltage of 40 kV and current of 20 mA. To characterize the phase composition of the sintered sample, a diffractometer (Empyrean, Panalytical) with a radiation source of Cu was used, operating with voltage of 45 kV and current of 40 mA. The microscopy analysis was carried out in a scanning electron microscopy (SEM) (Quanta FEG650, FEI) equipped with energy-dispersive X-ray spectroscopy (EDS) (Quantax, Bruker).

2.4 Physical and mechanical characterization

The density evaluation was based on ABNT NBR ISO 10545-3 (2017) following Archimedes' principle. The experimental density (ρ_{exp}), Eq. (1), was performed using a precision scale (model 200 CE, Marte), and a hydrostatic kit. First, the dry mass (m_1) was measured. Next, the sample was subject to boiling distilled water for 2 hours to impregnate the open pores. Then, the mass impregnated with water (m_2), and the suspended mass in distilled water (m_3) were measured.

$$\rho_{exp} = \frac{m_1}{m_2 - m_3} \cdot \rho_{H20} \; [g/cm^3] \tag{1}$$

The distilled water density (ρ_{H20}) was calculated according to Eq. (2), in which T is the distilled water temperature in [ºC] measured with a spit digital thermometer (model TM879, Equitherm) during the suspended mass step.

$$\rho_{H20} = 1,0017 - 0,0002135 \cdot T \; [^oC] \tag{2}$$

The theoretical density (ρ_{the}), Eq. (3), was obtained from the inverse rule of mixtures, using the weight percentages (wt%), and, from the powders datasheet, the specific density (ρ) (German and Park, 2008).

$$\frac{1}{\rho_{teor}} = \frac{wt\%_{Al2O3}}{\rho_{Al2O3}} + \frac{wt\%_{ZrO2}}{\rho_{ZrO2}} + \frac{wt\%_{SiCw}}{\rho_{SiCw}} \; [1/g/cm^3] \tag{3}$$

The relative density (ρ_{rel}), Eq. (4), is the ratio between the experimental density (ρ_{exp}), and the theoretical density (ρ_{the}) (ABNT NBR ISO 10545-3, 2017).

$$\rho_{rel} = \frac{\rho_{exp}}{\rho_{teor}} \cdot 100 \; [\%] \tag{4}$$

The Vickers hardness was conducted according to ASTM C1327 - 15 (2015) in a hardness tester (VMT-7, Buehler) with a load of 10 kgf. This load was chosen to generate cracks at the indentation vertex larger than their diagonals, allowing the measurement of the fracture toughness (Meyers and Chawla, 2009). The Vickers hardness number (HV) was calculated as shown in Eq. (5); in which P is the load in kgf and d the average length of diagonals in mm. The fracture toughness (K_{IC}) in mode I of loading was estimated as in Eq. (6), using Young's modulus (E) in GPa, Vickers hardness (H) in GPa, load (P) in N, and crack extension (c) in m.

$$HV = 1.8544 \frac{P}{d^2} \; [HV] \tag{5}$$

$$K_{IC} = 0.016 \left(\frac{E}{H}\right)^{1/2} \frac{P}{c^{3/2}} \; [MPa.m^{1/2}] \tag{6}$$

3. RESULTS

3.1 Sintering

Since the PECS machine is able to monitor the process variables, the temperature (red line), pressure (blue), and displacement (green) data of the sample during sintering is shown in Fig. 1. Classical stages of sintering can be noted, such as adhesion, initial, intermediate and final. Between minutes 0 and 6 there is only an accommodation of the powder with an increase of the contact surface among particles, due to the application of a uniaxial pressure of 50 MPa, characterizing the adhesion stage. The thermal cycle begins from the 6^{th} minute. In this stage, the neck formation among the particles is expected, with a reduction in the surface area. The greatest densification is observed between 12 and 20 minutes, in

the intermediate stage. As the heat increases at a rate of approximately 100°C/min, a fast and increasing displacement occurs. At this moment, according to the literature, tubular, rounded, and elongated pores are expected. The final stage is expected to initiate at the thermal plateau, around minute 20, and finish at the end of the cycle. In this stage there is pore closing, grain growth, and small densification. After the thermal plateau, a new little displacement is observed due to the thermal contraction as a cooling result. A slight swelling is observed at the very end of the pressure cycle, due to the mechanical relief of load on the punches (German, 1996). The advanced ceramic sample reached a total displacement (shrinkage) of 10.14 mm, indicating densification, in a cycle of 36 minutes.

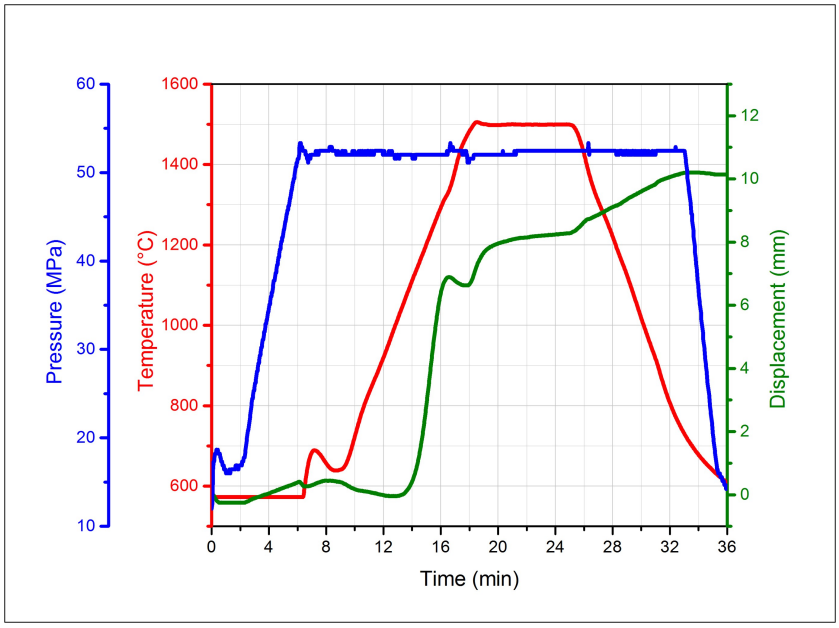

Figure 1. PECS sintering curves.

3.2 XRD and microscopic analysis

The mixed powder (Al_2O_3-ZrO_2-SiC_w) was analysed by XRD. The result is presented in Fig. 2. It is possible to identify all the phases present in the composite analysing the different peaks. α-Al_2O_3 stands out at 15.96°, 19.57° and 25.57°, β-SiC_w at 16.23° and 26.59°, tetragonal zirconia (t-ZrO_2) at 13.72° and 22.59°, and, finally, monoclinic zirconia (m-ZrO_2) at 12.94° and 14.24°.

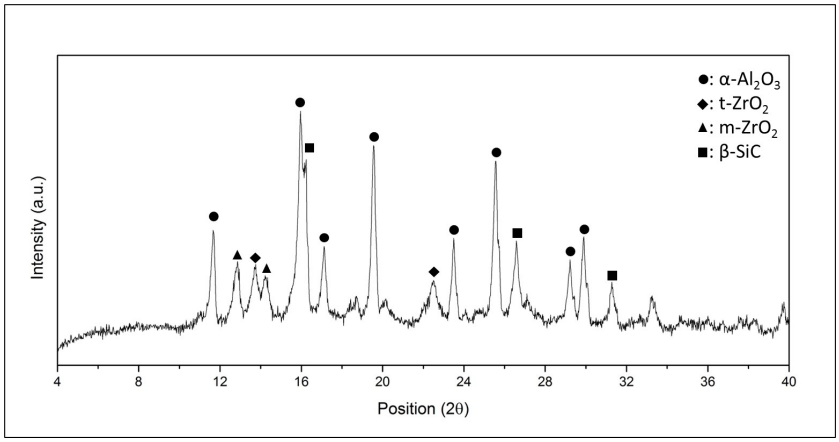

Figure 2. XRD of the mixed powder (Al_2O_3-ZrO_2-SiC_w).

The XRD of the sintered sample is presented in Fig. 3. The detected phases match those of the mixed powders. The highest peaks are α-Al_2O_3 at the position of 35.17°, 43.36°, 57.49° and 68.20°. SiC was detected at 35.75°, 60.08° and 71.98°. Owing to the temperature of sintering and the allotropic transformation that the stabilized zirconia undergoes, only the presence of t-ZrO_2 in the sample was expected after sintering (Boniecki *et al.*, 2017). However, it is possible to observe

the presence of m-ZrO_2, even with low intensity at positions 28.28°, 31.51° and 55.53°. This may have been caused by the residual stress, generated by the difference between moduli of elasticity and coefficient of thermal expansion among the constituents, particularly the β-SiC_w phase. t-ZrO_2 was detected in two peaks, also of low intensity, at positions 30.22° and 50.21°.

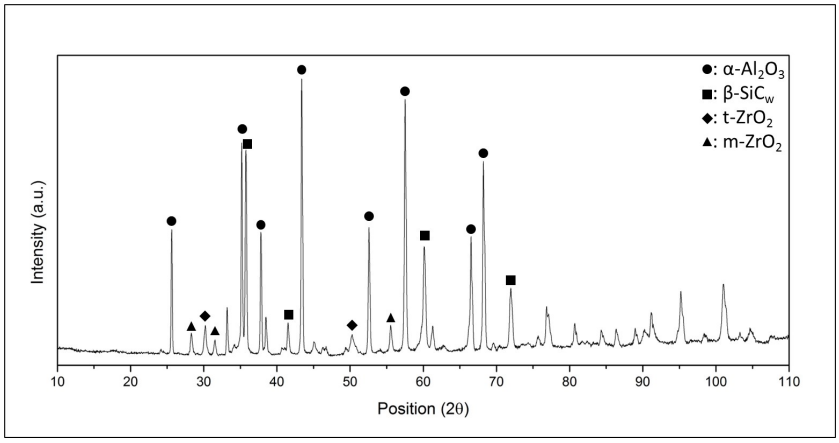

Figure 3. XRD of the sintered sample.

In Figure 4, the different phases of the sintered advanced ceramic can be seen. ZrO_2 phase, in green, is distributed in the Al_2O_3 matrix, in blue; in addition, some particles and fiber of SiC can be seen in orange. A larger presence of whiskers fiber was expected; however, the SiC powder used for sintering seems to have more particles than fibers. The presence of some pores was also observed. The porosity may be attributed to the sintering parameters that were not enough to provide full densification. However, some authors have pointed out the SiC_w influence to reduce higher densification by pinning on the grain boundary blocking mass transport or due to its covalent bond, which is more difficult to sinter (Zhang *et al.*, 2021; Grigoriev *et al.*, 2017).

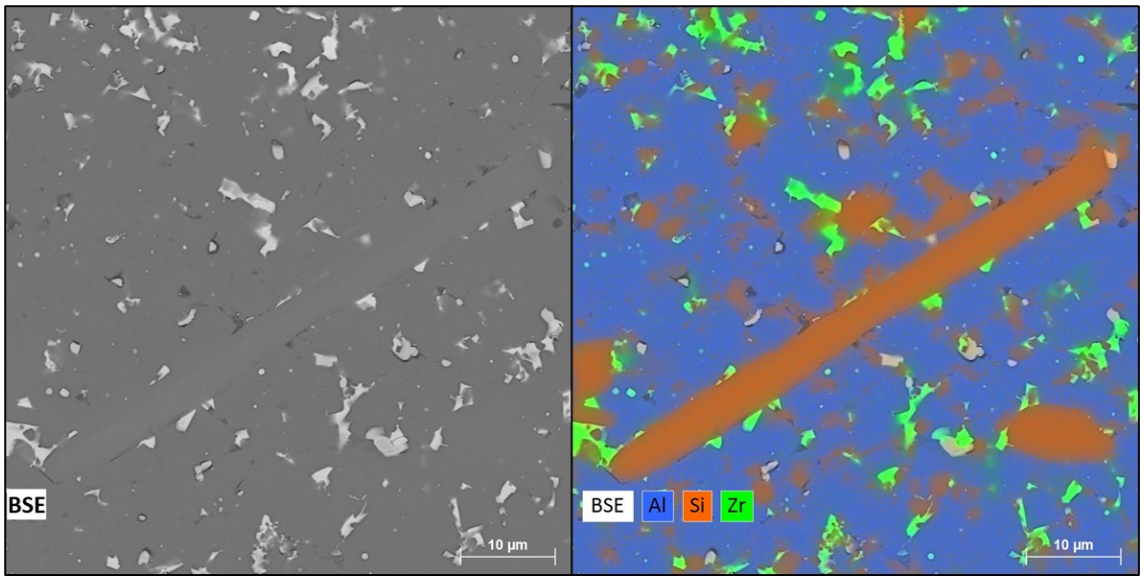

Figure 4. SEM and EDS of the advanced ceramic after sintering showing the different phases.

3.3 Physical and mechanical characterization

Density is an important parameter to characterize sintered materials, because it is directly related to the kinetics of sintering (German, 1996). The theoretical density of the advanced ceramic was 4.01 g/cm^3, while the experimental density, obtained from the average of 15 measurements, was 3.84 ± 0.02 g/cm^3. The ratio between both densities resulted in a relative density of 95.83 ± 0.47 %. Tamura *et al.* (2018) sintered samples of Al_2O_3 by PECS using different temperatures and times. The samples sintered at 1300°C and 5 or 10 min dwell time, and the samples sintered at 1400°C with

a dwell time of less than 5 min reached 100% of relative density. Gao *et al.* (1999) evaluated the density of 80%Al_2O_3-15%(3Y)ZrO_2-5%SiC samples sintered by PECS using temperatures between 1350°C and 1600°C, heating and cooling rate of 600°C and without dwell time. The sample sintered at 1450°C almost reached full densification. Zhang *et al.* (2020) invesigated the addition of SiC_w to a ZrO_2-20%volAl_2O_3 composite sintered by oscilatory pressure. During the thermal dwell of 1550°C the total pressure varied between 27.5 and 32.5 MPa. Regardless of the amount of SiC present, all samples exhibited high relative density, higher than 98%.

Figure 5 shows the Vickers hardness number values of eight indentations, and average with standard deviation.

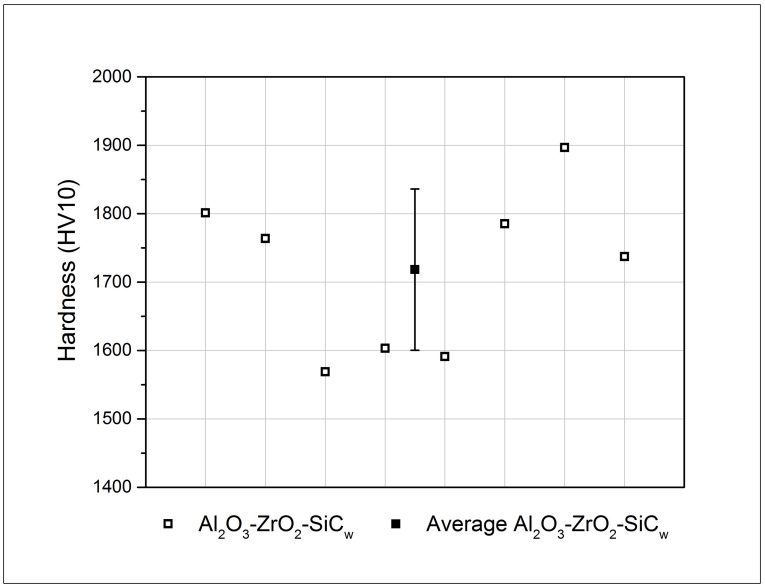

Figure 5. Vickers hardness number result.

The average Vickers hardness number for the advanced ceramic was 1718.25 ± 118.02 HV10 (16.85 ± 1.16 GPa), which is close to the literature values for similar compositions. Kumar *et al.* (2006) highlighted the properties of ceramic cutting tools. Among them, for 96.5% Al_2O_3 and 3.5% ZrO_2 ceramic composite the Vickers hardness attributed was 1730 HV. However, for the tool composed of 80% Al_2O_3 and 20% SiC_w, the hardness was 2000 HV, indicating that the addition of SiC_w improved the mechanical property. Chen *et al.* (2015) manufactured samples of α-Al_2O_3-based by PECS at 1400°C. The characterization showed that the monolithic alumina had the higher hardness 1835 HV (18 GPa). Gutiérrez-González *et al.* (2016) fabricated an Al_2O_3-SiC_w sample by PECS at 1780°C and 30 MPa. The hardness analysis showed a maximum value of 1616.19 HV (15.85 GPa).

Figure 6 shows the fracture toughness (K_{IC}) values for eight observations, and average with standard deviation.

The advanced ceramic sample reached (K_{IC}) of 3.69 ± 0.57 MPa.m$^{1/2}$. Chen *et al.* (2015) obtained a value around 3.5 MPa.m$^{1/2}$ for monolithic alumina sintered by PECS. Kumar *et al.* (2006) presented K_{IC} values of 4.5 and 8 MPa.m$^{1/2}$ for a cutting tool composed of 96.5% Al_2O_3 and 3.5% ZrO_2 and 80% Al_2O_3 and 20% SiC_w, respectively. Bertolete *et al.* (2020) showed a value of 5.17 ± 0.56 MPa.m$^{1/2}$ for a homogeneous Al_2O_3–30vol%ZrO_2 sintered by PECS. The fracture toughness value obtained is comparable with similar ceramics in the literature, although a higher value was expected due to the addition of the SiC whiskers. The difference is related to particle size, volume fraction, sintering conditions, and sintering technique.

4. CONCLUSION

The results indicated the viability of manufacturing Al_2O_3-based ceramics with good densification and mechanical properties in a short time by PECS. Although the advanced ceramic sample reached 95.83 ± 0.47% of relative density, it can be improved by optimizing the sintering parameters that will influence the mechanical properties. The XRD analysis showed the presence of monoclinic zirconia in the sintered sample, probably due to internal residual stress. The MEV/EDS analysis showed the different phases with a good concentration of particles rather than SiC whiskers, besides the presence of porosity. The sample reached high hardness of 1718.25 ± 118.02 HV10. The fracture toughness (K_{IC}) of the ceramic was computed as 3.69 ± 0.57 MPa.m$^{1/2}$, lower than expected, probably due to the greater presence of particles than fibers of SiC. Finally, all the properties of the sample indicate the possibility of its use as a cutting tool; however, sintering adjustments and machining tests should be conducted to validate its application.

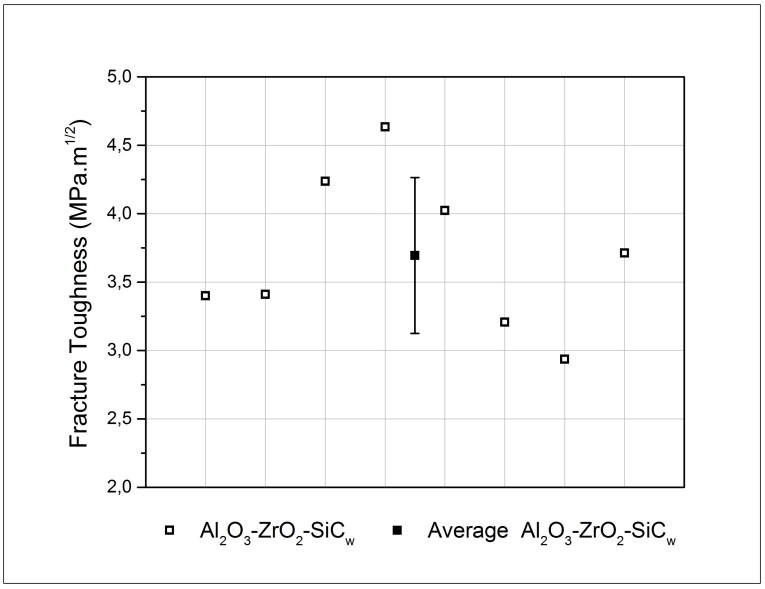

Figure 6. Fracture toughness (K_{IC}) result.

5. ACKNOWLEDGEMENTS

The authors thank the FAPES (processes 083/2019, 108/2021, and 1066/2022) for research support, CNPq and CAPES.

6. REFERENCES

ABNT NBR ISO 10545-3, 2017. *Placas cerâmicas - Parte 3: Determinação da absorção de água, porosidade aparente, densidade relativa aparente e densidade aparente*. Rio de Janeiro.

ASTM C1327 - 15, 2015. *Standard Test Method For Vickers Indentation Hardness of Advanced Ceramics*. West Conshohocken.

Bertolete, M., Barbosa, P., De Rossi, W., Fredericci, C. and Machado, I., 2020. "Mechanical characterisation and machining evaluation of ceramic cutting tools functionally graded with six layers". *Ceramics International*, Vol. 46, No. 10, pp. 15137–15145.

Boniecki, M., Gołębiewski, P., Wesołowski, W., Woluntarski, M., Piątkowska, A., Romaniec, M., Ciepielewski, P. and Krzyżak, K., 2017. "Alumina/zirconia composites toughened by the addition of graphene flakes". *Ceramics International*, Vol. 43, No. 13, pp. 10066–10070.

Casto, S.L., Valvo, E.L., Lucchini, E., Maschio, S. and Ruisi, V., 1997. "Wear rates and wear mechanisms of alumina-based tools cutting steel at a low cutting speed". *Wear*, Vol. 208, No. 1-2, pp. 67–72.

Chai, J., Zhu, Y., Wang, Z., Shen, T., Liu, Y., Niu, L., Li, S., Yao, C., Cui, M. and Liu, C., 2020. "Microstructure and mechanical properties of SPS sintered Al_2O_3–ZrO_2 (3Y)–SiC ceramic composites". *Materials Science and Engineering: A*, Vol. 781, p. 139197.

Chakravarty, D. and Sundararajan, G., 2013. "Microstructure, mechanical properties and machining performance of spark plasma sintered Al_2O_3–ZrO_2–TiCN nanocomposites". *Journal of the European Ceramic Society*, Vol. 33, No. 13-14, pp. 2597–2607.

Chen, W.H., Lin, H.T., Nayak, P.K., Chang, M.P. and Huang, J.L., 2015. "Sintering behavior and mechanical properties of WC–Al_2O_3 composites prepared by spark plasma sintering (SPS)". *International Journal of Refractory Metals and Hard Materials*, Vol. 48, pp. 414–417.

Fang, Y., Chen, N., Du, G., Zhang, M., Zhao, X. and Wu, J., 2019. "Effect of Y_2O_3-stabilized ZrO_2 whiskers on the microstructure, mechanical and wear resistance properties of Al_2O_3 based ceramic composites". *Ceramics International*, Vol. 45, No. 13, pp. 16504–16511.

Gao, L., Wang, H., Hong, J., Miyamoto, H., Miyamoto, K., Nishikawa, Y. and Torre, S., 1999. "SiC-ZrO_2 (3Y)-Al_2O_3 nanocomposites superfast densified by spark plasma sintering". *Nanostructured materials*, Vol. 11, No. 1, pp. 43–49.

German, R.M., 1996. *Sintering theory and practice*. John Wiley & Sons Inc., New York. 558 p.

German, R.M. and Park, S.J., 2008. *Mathematical Relations in Particulate Materials Processing: Ceramics, Powder Metals, Cermets, Carbides, Hard Materials, and Minerals*. John Wiley & Sons, Hoboken. 419 p.

Gevorkyan, E., Rucki, M., Panchenko, S., Sofronov, D., Chałko, L. and Mazur, T., 2020. "Effect of sic addition to Al_2O_3 ceramics used in cutting tools". *Materials*, Vol. 13, No. 22, p. 5195.

Gong, F., Zhao, J., Li, Z., Sun, J., Ni, X. and Hou, G., 2018. "Design, fabrication and mechanical properties of multidimensional graded ceramic tool materials". *Ceramics International*, Vol. 44, No. 3, pp. 2941–2951.

Grigoriev, S., Peretyagin, P., Smirnov, A., Solis, W., Díaz, L.A., Fernández, A. and Torrecillas, R., 2017. "Effect of graphene addition on the mechanical and electrical properties of Al_2O_3-SiC_w ceramics". *Journal of the European ceramic society*, Vol. 37, No. 6, pp. 2473–2479.

Gutiérrez-González, C.F., Suárez, M., Pozhidaev, S., Rivera, S., Peretyagin, P., Solís, W., Díaz, L.A., Fernández, A. and Torrecillas, R., 2016. "Effect of TiC addition on the mechanical behaviour of Al_2O_3–SiC whiskers composites obtained by SPS". *Journal of the European Ceramic Society*, Vol. 36, No. 8, pp. 2149–2152.

Kumar, A.S., Durai, A.R. and Sornakumar, T., 2006. "The effect of tool wear on tool life of alumina-based ceramic cutting tools while machining hardened martensitic stainless steel". *Journal of Materials Processing Technology*, Vol. 173, No. 2, pp. 151–156.

Ma, F., Huang, C., Niu, J., Wang, L., Liu, H. and Bai, X., 2022. "Toughening mechanisms of Al_2O_3-matrix composites with SiC whiskers". *Ceramics International*, Vol. 48, No. 12, pp. 17556–17563.

Meyers, A.M. and Chawla, K.K., 2009. *Mechanical behavior of materials*. Cambridge University Press, Cambridge, 2nd edition. 882 p.

Moghanlou, F.S., Vajdi, M., Sha, J., Motallebzadeh, A., Shokouhimehr, M. and Asl, M.S., 2019. "A numerical approach to the heat transfer in monolithic and SiC reinforced HfB_2, ZrB_2 and TiB_2 ceramic cutting tools". *Ceramics International*, Vol. 45, pp. 15892–15897.

Orru, R., Licheri, R., Locci, A.M., Cincotti, A. and Cao, G., 2009. "Consolidation/synthesis of materials by electric current activated/assisted sintering". *Materials Science and Engineering: R: Reports*, Vol. 63, No. 4-6, pp. 127–287.

Otitoju, T.A., Okoye, P.U., Chen, G., Li, Y., Okoye, M.O. and Li, S., 2020. "Advanced ceramic components: Materials, fabrication, and applications". *Journal of industrial and engineering chemistry*, Vol. 85, pp. 34–65.

Ranjan, P. and Hiremath, S.S., 2019. "Role of textured tool in improving machining performance: A review". *Journal of Manufacturing Processes*, Vol. 43, pp. 47–73.

Tamura, Y., Zapata-Solvas, E., Moshtaghioun, B.M., Gomez-Garcia, D. and Dominguez-Rodriguez, A., 2018. "Grain-boundary diffusion coefficient in α-Al_2O_3 from spark plasma sintering tests: Evidence of collective motion of charge disconnections". *Ceramics International*, Vol. 44, No. 15, pp. 19044–19048.

Zhang, J., Zhu, T., Cheng, Y., Sang, S., Li, Y., An, D. and Xie, Z., 2020. "Fabrication and mechanical properties of ZrO_2–Al_2O_3–$SiC_{(w)}$ composites by oscillatory pressure sintering". *Ceramics International*, Vol. 46, No. 16, pp. 25719–25725.

Zhang, J., Zhu, T., Sang, S., Li, Y., Pan, L., Liao, N., Liang, X., Wang, Q., Xie, Z. and Dai, J., 2021. "Microstructural evolution and mechanical properties of ZrO_2 (3Y)–Al_2O_3–$SiC_{(w)}$ ceramics under oscillatory pressure sintering". *Materials Science and Engineering: A*, Vol. 819, p. 141445.

Zhang, Z., Liu, Y. and Liu, H., 2022. "Mechanical properties and microstructure of spark plasma sintered Al_2O_3-SiC_w-Si_3N_4 composite ceramic tool materials". *Ceramics International*, Vol. 48, No. 4, pp. 5527–5534.

7. RESPONSIBILITY NOTICE

The authors are solely responsible for the printed material included in this paper.